Neurobiology of Disease 49 (2013) 221–231

Contents lists available at SciVerse ScienceDirect

Neurobiology of Disease

journal homepage: www.elsevier.com/locate/ynbdi

An essential role of MAG in mediating axon–myelin attachment in Charcot–Marie–Tooth 1A disease

Jochen Kinter [a], Thomas Lazzati [a], Daniela Schmid [a], Thomas Zeis [a], Beat Erne [a], Roland Lützelschwab [a,b,1], Andreas J. Steck [a,b], Davide Pareyson [c], Elior Peles [d], Nicole Schaeren-Wiemers [a,b,*]

[a] Neurobiology, Department of Biomedicine, University Hospital Basel, University of Basel, Hebelstrasse 20, CH-4031 Basel, Switzerland
[b] Department of Neurology, University Hospital Basel, University of Basel, Hebelstrasse 20, CH-4031 Basel, Switzerland
[c] IRCCS Foundation, C. Besta Neurological Institute, Milan, Italy
[d] Department of Molecular Cell Biology, The Weizmann Institute of Science, POB 26, Rehovot 76100, Israel

ARTICLE INFO

Article history:
Received 8 June 2012
Revised 30 July 2012
Accepted 16 August 2012
Available online 25 August 2012

Keywords:
Myelin associated protein (MAG)
Nectin-like protein (Necl4)
Peripheral neuropathy
CMT1A
Axonal pathology

ABSTRACT

Charcot–Marie–Tooth disease type 1A (CMT1A) is a hereditary demyelinating peripheral neuropathy caused by the duplication of the PMP22 gene. Demyelination precedes the occurrence of clinical symptoms that correlate with axonal degeneration. It was postulated that a disturbed axon–glia interface contributes to altered myelination consequently leading to axonal degeneration. In this study, we examined the expression of MAG and Necl4, two critical adhesion molecules that are present at the axon–glia interface, in sural nerve biopsies of CMT1A patients and in peripheral nerves of mice overexpressing human PMP22, an animal model for CMT1A. We show an increase in the expression of MAG and a strong decrease of Necl4 in biopsies of CMT1A patients as well as in CMT1A mice. Expression analysis revealed that MAG is strongly upregulated during peripheral nerve maturation, whereas Necl4 expression remains very low. Ablating MAG in CMT1A mice results in separation of axons from their myelin sheath. Our data show that MAG is important for axon–glia contact in a model for CMT1A, and suggest that its increased expression in CMT1A disease has a compensatory role in the pathology of the disease. Thus, we demonstrate that MAG together with other adhesion molecules such as Necl4 is important in sustaining axonal integrity.

Introduction

Generation of functional myelinated nerves requires a reciprocal communication between myelinating cells and their associated axons. Myelination is established by highly specialized glial cells, oligodendrocytes in the central nervous system and Schwann cells in the peripheral nervous system (PNS) that wrap axons with a multilayered myelin membrane for rapid impulse conduction. In addition, axonal signals regulate the survival, migration and differentiation of Schwann cells as well as the myelination process (Jessen and Mirsky, 2005; Nave and Salzer, 2006; Nave and Trapp, 2008). Recent studies have shown that axon–glia contact is mediated by different adhesion molecules that are located at and around the nodes of Ranvier (Eshed et al., 2005; Gollan et al., 2003; Poliak et al., 1999) or along the internode (Maurel et al., 2007; Spiegel et al., 2007; Trapp, 1990). The myelin associated glycoprotein (MAG) is expressed in the periaxonal glial membrane at initial stages of myelination (Martini and Schachner, 1986) and interacts with several axonal components (Hannila et al., 2007). At later stages of myelination, MAG is localized to Schmidt–Lanterman incisures as well (Trapp, 1990). However, mice deficient in MAG myelinate appropriately and exhibit only modest alterations in the periaxonal space (Li et al., 1994; Montag et al., 1994), suggesting that other adhesion molecules such as N-CAM and L1 (Bartsch, 2003) or the recently identified Nectin-like protein 4 (Necl4) protein (Maurel et al., 2007; Spiegel et al., 2007) are likely to contribute in axon–glial adhesion along the internode. Necl4 is located at the Schwann cell–axon interface, where it interacts with the axonal Necl1 (Maurel et al., 2007; Spiegel et al., 2007). Its localization within the different compartments of the peripheral myelin sheath is highly similar to MAG (Maurel et al., 2007; Spiegel et al., 2007), but a functional relationship between the two adhesion proteins is not yet known.

Charcot–Marie–Tooth disease (CMT) is the most frequent hereditary peripheral neuropathy. The CMT1A subtype is classified as a primary demyelinating disease and affects about 70–80% of all CMT1 cases

* Corresponding author at: Neurobiology, Department of Biomedicine, University Hospital Basel, Hebelstrasse 20, Switzerland, CH-4031 Basel, Switzerland.
E-mail addresses: j.kinter@unibas.ch (J. Kinter), thomas.lazzati@unibas.ch (T. Lazzati), daniela.schmid@unibas.ch (D. Schmid), thomas.zeis@unibas.ch (T. Zeis), beat.erne@unibas.ch (B. Erne), roland.luetzelschwab@roche.com (R. Lützelschwab), asteck@uhbs.ch (A.J. Steck), davide.pareyson@istituto-besta.it (D. Pareyson), peles@weizmann.ac.il (E. Peles), nicole.schaeren-wiemers@unibas.ch (N. Schaeren-Wiemers).
Available online on ScienceDirect (www.sciencedirect.com).
[1] Present address: F. Hoffmann-La Roche Ltd., Basel, Switzerland.

0969-9961/$ – see front matter © 2012 Elsevier Inc. All rights reserved.
http://dx.doi.org/10.1016/j.nbd.2012.08.009

(Schenone and Mancardi, 1999). Generally speaking CMT1A genes encode proteins involved in myelination, highlighting the fact that Schwann cells in the PNS is the primary site of pathology (Nelis et al., 1996). However, even in this situation, an axonopathy is also found (Krajewski et al., 2000), suggesting that axon–glial interactions may be critically involved. Because MAG and Necl4 are two important adhesion molecules that are present at the axon–glia interface we expected that they could play a critical role in the pathogenesis of this condition. CMT1A leads to distal weakness, atrophy and sensory loss caused by degeneration of motor and sensory axons (Krajewski et al., 2000). Demyelination precedes the occurrence of clinical symptoms that correlate with axonal degeneration (Berciano et al., 1989; Bouche et al., 1983; Garcia et al., 1998; Nicholson, 1991). CMT1A is caused by duplication of the DNA region encoding the peripheral myelin protein 22 (PMP22) or by a point-mutation within this gene (Patel et al., 1992; Roa et al., 1991; Suter et al., 1992). To analyze the role of altered PMP22 in disease progression several animal models have been generated (Huxley et al., 1996; Sereda and Nave, 2006). Studies using these models have revealed that overexpression of PMP22 disturbs Schwann cell maturation and causes metabolic perturbations, resulting in axonal dysfunction (de Waegh et al., 1992; Nagarajan et al., 2001; Srinivasan et al., 2007). It was postulated that a disturbed axon–glia interaction might contribute to altered myelination, consequently leading to axonal degeneration (Martini, 2001). Herein, we examined the role of MAG and Necl4 in the axonal pathology of CMT1A by investigating human nerve biopsies and peripheral nerves of a particular mouse model, the C22 mouse line, which overexpresses human PMP22 (Huxley et al., 1996).

Material and methods

Patients and control subjects

Human tissue (sural nerves) was obtained from biopsies (after written informed consent was obtained, approved by the local advisory board) and autopsies (kindly provided by Dr. A. Probst, Neuropathology, University Hospital Basel, Switzerland). Sural nerves obtained at autopsy from three patients (two male and one female, Supplementary Fig. 1G) without any diagnosed neurological disease were taken as controls (with permission by the Ethics Committee of the University Hospital Basel). These subjects had an average age of 86 years (±5.1 standard error of the mean (s.e.m.) and the average post mortem time of autopsy was 5.3 h (±1.2 s.e.m.). Sural nerve biopsy tissues from three CMT1A and five HNPP patients were used in this study (Supplementary Fig. 1G) (Gabriel et al., 1997). In the three CMT1A patients (two females and one male) motor conduction velocity ranged between 10 and 22 m/s and the average age at biopsy was 24.3 years (±21.0 s.e.m.). The five HNPP patients (one female and four males) had a motor conduction velocity ranging between 33 and 56 m/s, and the average age at biopsy was 28.2 years (±12.1 s.e.m.). Confocal colocalization microscopy for Necl4 and MAG was performed with control patient BA63 (46 years old, 15 h post mortem, infarct) and CMT1A patients mi5 and mi6 (Supplementary Fig. 1G).

Antibodies

Primary antibodies for Western blot analysis

Anti-MAG (polyclonal, kindly provided by Dr. A.M. Heape, Oulu University and Central Hospital, Finland), anti-MBP (MAB386, Chemicon), anti-P0 (kindly provided by Dr. J.J. Archelos, Karl-Franzens University, Graz, Austria), anti-mouse PMP22 (kindly provided by Dr. U. Suter, ETH-Hönggerberg, Zürich, Switzerland), anti-CNPase (clone SMI91, Covance), anti-Necl1 and anti-Necl4 (Spiegel et al., 2007) were used.

Secondary antibodies for Western blot analysis

Goat anti-mouse Alexa Fluor 680, goat anti-rabbit IRDye 800 (LI-COR Biosciences GmbH) and goat anti-rat IRDye 800 (Rockland) were used.

Primary antibodies for immunohistochemistry

Anti-human MAG (specific for extracellular epitope, D3A2G5 Burger et al., 1990), anti-human L-MAG (Miescher et al., 1997), anti-human S-MAG (Miescher et al., 1997), anti-human P0 (clone D4IE4 Miller et al., 1984), anti-mouse MAG (clone 513, Boehringer Mannheim), anti-mouse PMP22 (see above), anti-mouse Necl4 (Spiegel et al., 2007), anti-mouse Caspr (Spiegel et al., 2007), pan anti-Nav (S-8809, Sigma) were used.

Secondary antibodies for immunohistochemistry

Goat anti-mouse and goat anti-rabbit peroxidase antibodies (Sigma), goat anti-mouse Alexa 555, goat anti-mouse Alexa 488 and goat anti-rabbit Alexa 488 (Molecular Probes), goat anti-rabbit Cy3 and goat anti-mouse Cy3 (Jackson ImmunoResearch Europe) were used.

Mice

The PMP22 overexpressing mice (line C22, kindly provided by Dr. C. Huxley, Imperial College School of Science, London, UK) carry seven copies of the human PMP22 gene (YAC construct) resulting in a peripheral neuropathy closely reflecting the CMT1A pathology observed in humans (Huxley et al., 1996). MAG-deficient mice (Montag et al., 1994) were kindly provided by Dr. K.A. Nave (MPI Göttingen, Germany). MAG-deficient mice were crossbred with C22 mice in our animal facility and survival of this new transgenic line was scored. The weight comparison between genotypes was performed at six weeks of age. Standard deviation (s.d.) was used to depict the variation occurring in the sample. The Kaplan–Meier estimator depicts the reduced life expectancy of the C22xMAG−/− double mutant for the first three months of 35 animals. Genotypes were determined by PCR using genomic DNA derived from ear piercing or tail biopsies. All mice were kept under standard SPF-conditions, housed and treated according to the guidelines for care and use of experimental animals of Veterinary Office of the Canton of Basel.

Immunohistochemistry

Consecutive cryostat sections of 10 μm were mounted on slides coated with Chrome Alum Gelatin. Fixation, delipidation and staining were performed as described previously (Gabriel et al., 1997). The blocking buffer for mouse tissues was PBS containing 0.1% fish skin gelatin, 2.5% normal goat serum, and 0.05% Saponin. Detection was performed with secondary horseradish peroxidase coupled antibodies (mouse or rabbit, respectively). Cell nuclei were counterstained with Mayer's Haemalaun (Merck). For immunofluorescence analysis, slides were incubated with secondary fluorophore-labeled antibodies as previously described. For immunohistochemistry analysis sections were mounted with Kaiser's glycerol gelatine (Merck); for immunofluorescence FluorSave Reagent (Calbiochem) was used as mounting and anti-fading medium.

Quantitative image analysis

Human sural nerve, transversal section

Quantifications of MAG expression were performed with biopsies from three CMT1A and five HNPP patients and three control autopsies. Ten test fields (11,011 μm^2 each) per section were analyzed using a Leica Dialux 20 microscope (Leitz) to evaluate the number of fibers positive for P0 and MAG. The degree of MAG expression was calculated as the ratio of the number of MAG positively stained fibers compared to P0 positively stained nerve fibers. On the same sections, areas stained for MAG and P0 were measured on 50 test fields with higher magnification (4439 μm^2 each) and the ratios of the quantified areas were calculated. Standard error of the mean (s.e.m.) was used to evaluate the difference between the means of the independent evaluation

performed. Cameras: JVC KY-F55, Olympus F-View; imaging software: "AnalySIS", Soft Imaging System.

Mouse sciatic nerve, transversal section

For the quantitative analysis of MAG expression, we performed a double staining for MAG and P0 or PMP22 on sciatic nerve transversal sections without counter stain. Sections from one C22 mouse and one wildtype littermate at postnatal day 20 (P20) were systematically analyzed acquiring three pictures with a 63× objective (oil, numeric aperture 1.32) with a resolution of 6.23 in/pixel on the light-transmission DMRE microscope (Leica). From each picture, fluorescent areas above background level of single myelinated fiber were evaluated by defining two circular areas of different sizes, to analyze large and small caliber fibers separately. The evaluated areas for 50 large (>5 μm) and 50 small (<5 μm) myelinated fibers in wildtype mice was compared with the intensities from 50 small myelinated fibers in C22 mice. Camera: Olympus F-View II; imaging software: "AnalySIS", Soft Imaging System.

Ultrastructural analysis, sampling strategy and quantification

Mice were deeply anesthetized with Isoflurane® (Abbott), decapitated and dissected rapidly. The tissue was either used directly or

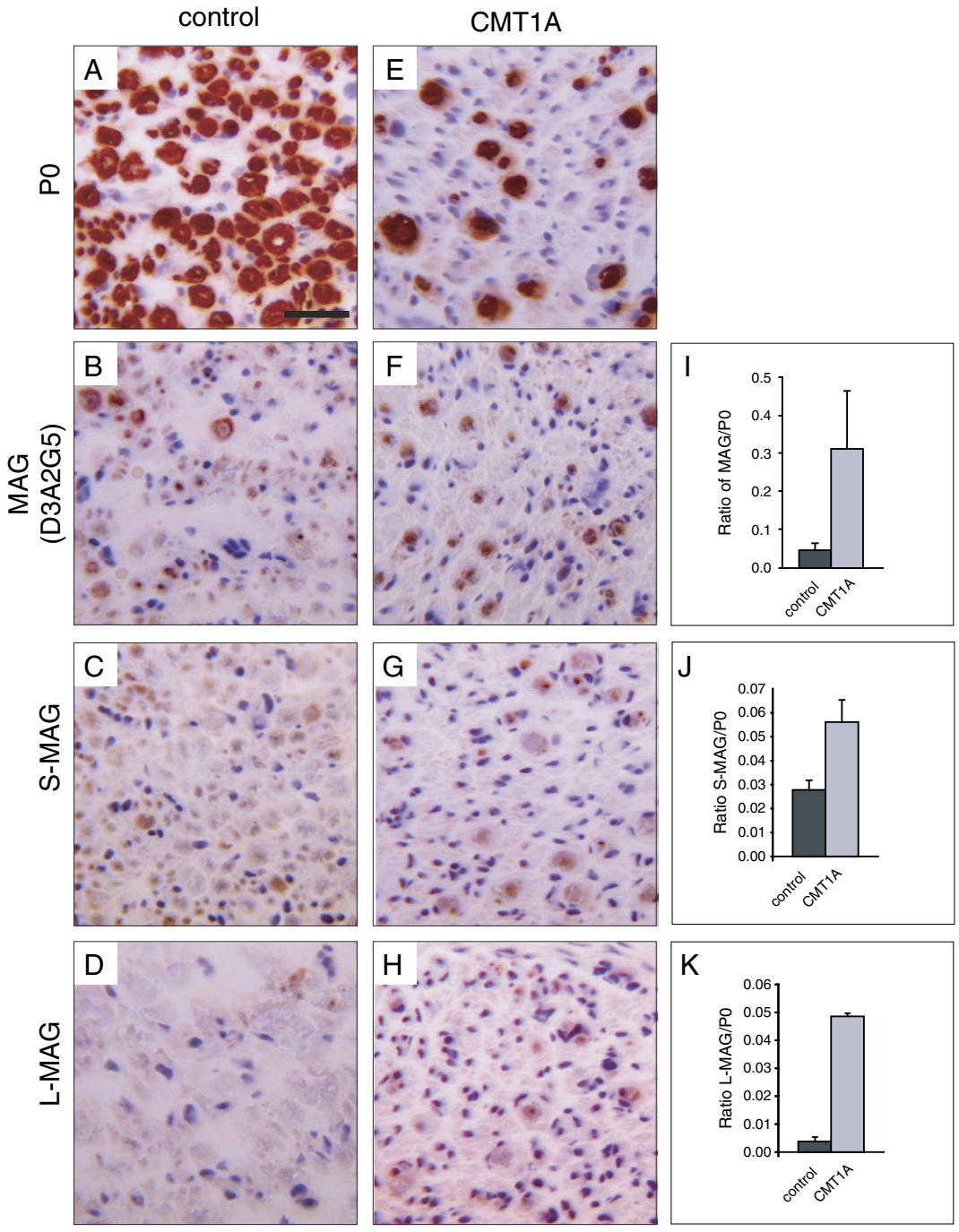

Fig. 1. MAG is induced in CMT1A patients. Transversal sections from sural nerves of control autopsies (A–D) and CMT1A biopsies (E–H) stained for P0 and MAG. Isoform specific antibodies recognizing S-MAG (C, G) or L-MAG (D, H) and an antibody recognizing both isoforms (B, F) were used. In CMT1A patients, the number of myelinated P0 positive fibers was reduced (E). However, the ratio of MAG-positive area relative to P0 positive area was higher in CMT1A patients than in control cases (I–K). The results of the quantitative measurements are expressed as mean and standard error of the mean (s.e.m.) in the bar graphs (single values are given in Supplementary Fig. 1I). Scale bar: 20 μm.

snap frozen on dry ice for quantitative Western blot analysis or embedded in O.C.T. compound (Sakura Finetek) and snap frozen on dry ice for immunohistochemistry. Tissue taken for electron microscopy (EM) was pre-fixed for 5 to 10 min by immersion in situ in a modified Karnovsky solution (3% glutaraldehyde, 3% paraformaldehyde in 0.1 M cacodylate buffer, Sigma). Nervous tissue was carefully excised and post-fixed in the same solution for 3–4 h at room temperature. Further post-fixation of the tissue pieces was performed in 2% glutaraldehyde in 0.1 M cacodylate buffer for at least 3 days at 4 °C. Postfixation with osmium tetroxide-potassium ferrocyanide (Polyscience inc. and Sigma), dehydration and Epon embedding (Sigma) were performed as described previously (Bartsch et al., 1995).

For the following sampling strategy and quantifications we always used three animals from each genotype: wildtype, C22, MAG−/− and C22xMAG−/− at P40. Semi-thin sections were performed for visual reconstruction of the whole tibial and peroneal branch of the sciatic nerve. Staining of semi-thin sections was performed by immersion of the slides in a solution of 1% of *p*-phenylenediamine (PPD, P6001, Sigma) dissolved in distilled water and double filtered with folded filter paper (LS-14, Schleicher & Schuell). The myelinated fibers were stained by immersion of the slides in PPD solution at room temperature for 10 min. Serial pictures were acquired on a light-transmission DMRE microscope (Leica) using a 63× objective (oil, numeric aperture 1.32) with a resolution of 6.23 in/pixel on pictures acquired with Olympus ColorView III. Pictures were stitched together to create an overview picture of the total area of the cross-sectioned nerve. The area of all nerve fascicles was measured.

For EM, the tibial and peroneal branches of the sciatic nerve were analyzed on a Morgagni 268D transmission electron microscope (Philips) with CCD camera (MegaView II, SIS). The two branches were systematically analyzed with 15–17 non-overlapping pictures each with a magnification of 2200× and the absolute number of myelinated axons per area was evaluated. A mean number of 5253 myelinated axons (±161 s.e.m.) was observed for wildtype mice, 2695 (±122 s.e.m.) for C22 mice and a mean of 3192 (±77 s.e.m.) for C22xMAG−/− mice. Axon–glia detachments were defined as regions where the membrane of the axon was

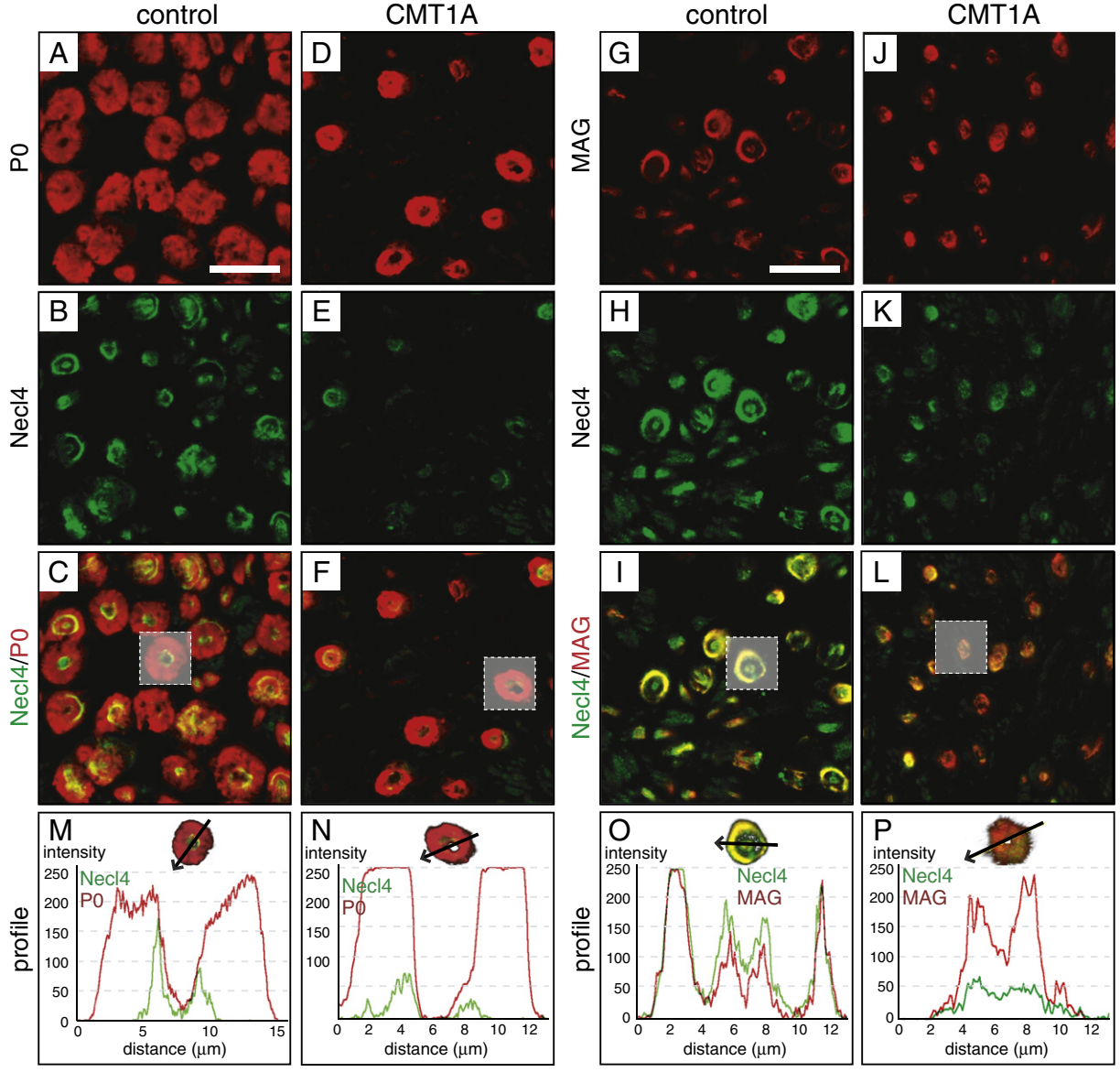

Fig. 2. Altered periaxonal localization of MAG and Necl4 in CMT1A patients. Immunofluorescent confocal colocalization of transversal sections from sural nerves of control autopsies (A–C, G–I) and CMT1A biopsies (D–F, J–L) for Necl4 (B, E, H, K) and either P0 (A, D) or MAG (G, J). Immunofluorescence for Necl4 was strongly decreased in nerve tissue from CMT1A patients (E, K, N, P). MAG and Necl4 were colocalized at periaxonal regions in control as well as in CMT1A patients (I, L, O, P). Analysis of fiber profiles revealed an altered ratio of immunolabeling for MAG and Necl4 at the periaxonal region in CMT1A patients (P). A reduction of Schmidt–Lanterman incisures in CMT1A is observed, which is due to the loss of large caliber fibers in CMT1A, which have many more Schmidt–Lanterman incisures than small caliber fibers. Scale bar: 20 μm.

not in direct contact with the membrane of the myelinating Schwann cell as assessed at a magnification of 22,000×. For this analysis a total number of 153–199 axons in an area of 2000 μm^2 were analyzed for axon–glia detachments, obtained from three independent pictures (magnification of 2200x) acquired from different region of the larger fascicle of the sciatic nerve from three C22 mice and three C22xMAG−/− mice. In wildtype and MAG−/− such phenomenon was never observed, and therefore not quantified. For C22xMAG−/− mice, the same 48 detached fibers were used to investigate the ratio of the inner to the total fiber diameter. Statistical evaluation of the differences in total number of myelinated axons and detachments was performed with two tailed Student's t-test. Longitudinal sections of sciatic nerve were acquired from region proximal to the ones analyzed in cross-sections.

Tissue preparation and Western blot analysis

The quantification of myelin proteins was performed with sciatic nerve myelin membrane preparations purified as described before (Schaeren-Wiemers et al., 2004). For each myelin preparation, sciatic nerves of eight adult animals were used. Myelin preparations were subjected to SDS-PAGE and analyzed by Western blot analysis. For whole sciatic nerve homogenates analysis, one sciatic nerve pair was homogenized in extraction buffer containing 50 mM Tris-buffer pH 7.4, 150 mM NaCl, 1% Triton X-100 supplemented with protease inhibitors (Roche Complete, EDTA-free) and phosphatase inhibitors (P5726, Sigma). Protein concentrations were determined either by Bradford or BCA assays and equal amount of protein was loaded on Tris-Glycine gels or NUPAGE precast gels (Invitrogen) and subjected to SDS–PAGE. Western blotting was performed as described previously (Schaeren-Wiemers et al., 2004).

Expression analysis

Total RNA was isolated from peripheral nerves from P0, P4, P7, P10 and P60 using QIAZOL Lysis Reagent (QIAGEN) and the RNeasy Micro Kit (QIAGEN) according to the manufacturer's protocol. RNA integrity was checked with the Agilent Bioanalyzer system. All RNA samples have an RNA integrity number (RIN) of above 8. RNA used for microarray analysis was amplified and biotinylated using the Illumina TotalPrep RNA Amplification Kit (Applied Biosystems) according to the manufacturer's protocol. Arrays were scanned using the iScan Reader (Illumina) and analyzed with the GenomeStudio software from Illumina. Gene expression was normalized to the global median. Microarray expression analysis was performed with 28 nerves from 14 mice pooled to seven experimental samples (n = 7) per genotype at P0 and P10, 20 nerves from 10 mice pooled to five experimental samples (n = 5)

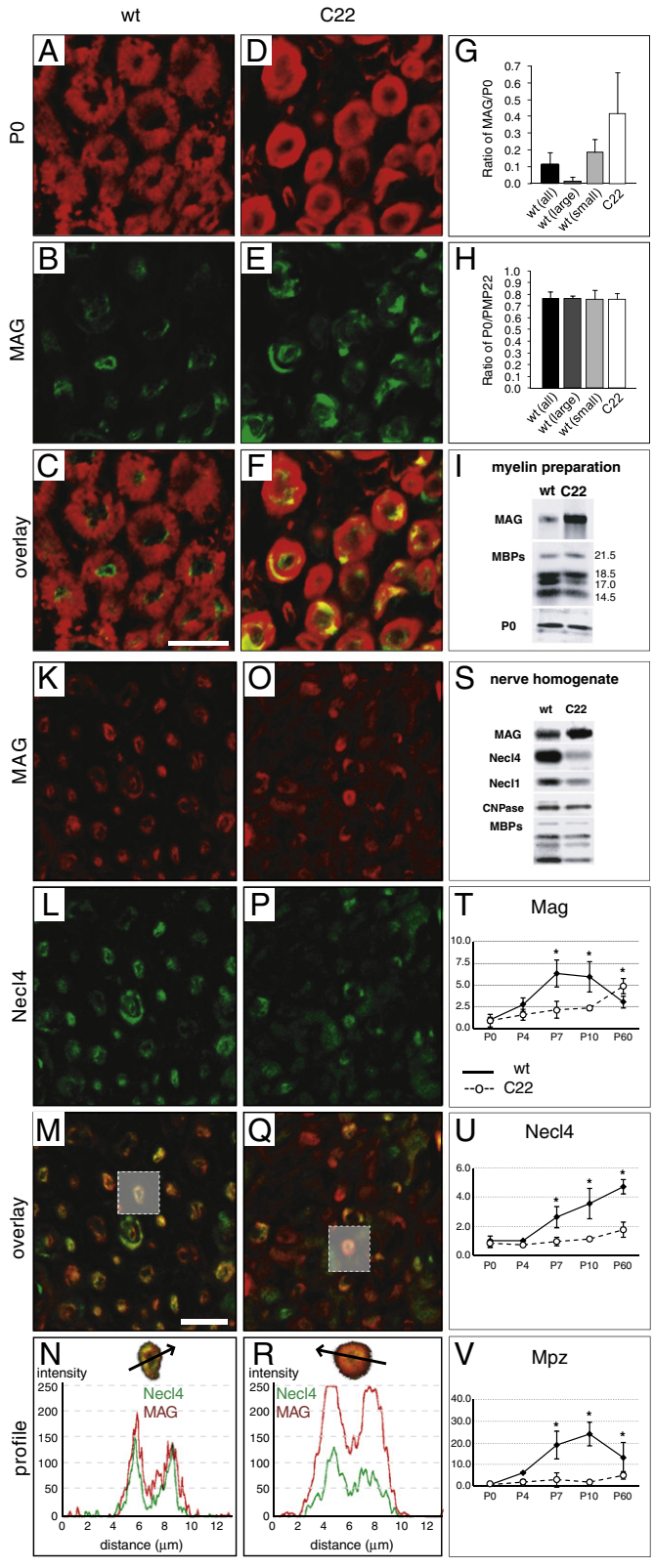

Fig. 3. MAG is increased and Necl4 reduced in a CMT1A animal model. Transversal sections from sciatic nerves of P60 wildtype (A–C) and C22 mice (D–F) stained for P0 (A, D) and MAG (B, E). The ratio of MAG/P0-positive areas was calculated from 50 large (>5 μm) as well as 50 small (<5 μm) caliber fibers in a wildtype and 50 small caliber fibers in a C22 animal, depicting an increase of MAG in C22 myelinated fibers (G). Investigation of the ratio of PMP22/P0-positive area did not reveal any differences (H). Western blot analysis of myelin membrane preparations revealed increased MAG levels in myelin membranes of sciatic nerves from five months old C22 mice (I). Scale bar: (A–F) 10 μm. Immunofluorescent confocal colocalization of transversal sections from sciatic nerves of P60 wildtype (K–M) and C22 mice (O–Q) for MAG (K, O) and Necl4 (L, P) revealed a strong decrease of Necl4 in sciatic nerves from C22 mice (P). MAG and Necl4 were colocalized at periaxonal regions in wildtype (M, N) as well as in C22 mice (Q, R). Analysis of fiber profiles revealed an altered ratio of immunofluorescence for MAG and Necl4 at the periaxonal region in C22 mice (R) resembling the observations from in CMT1A patients. Western blot analysis of sciatic nerve tissue extracts from six months old wildtype and C22 mice showed that the protein levels of both Necl4 and Necl1 were strongly reduced in nerve extracts of C22 mice in contrast to MAG (S). Additionally, a reduction of the myelin protein MBP was detected in extracts of C22 mice, whereas comparable expression levels could be detected for CNPase (S). Note that the increased MAG expression in C22 was less pronounced in whole nerve protein extracts than in myelin membrane preparations (I). Quantitative RT-PCR was performed for Mag (T), Necl4 (U) and Mpz/P0 (V) at P0, P4, P7, P10 and P60 from wildtype (closed squares) and C22 (open circles, dashed line) mice. The mRNA expression levels were normalized to 60S expression and to its wildtype P0 level, which was set to 1. Significant differences ($p<0.05$) are indicated with an asterisk. Expression data are shown as mean and s.d. Scale bar: (K–Q) 20 μm.

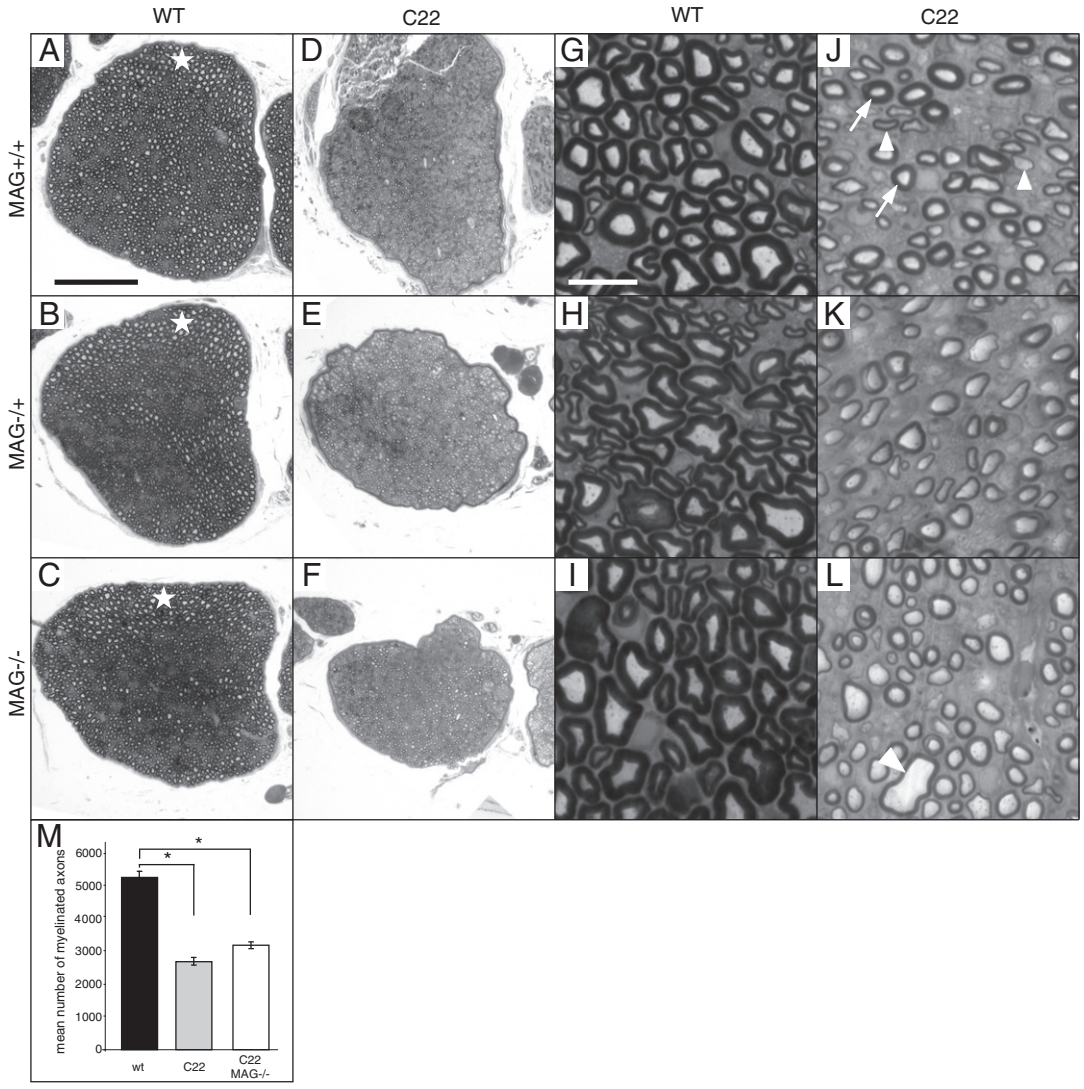

Fig. 4. MAG deficiency in C22 does not influence myelination. Myelination was analyzed by transversal section of sciatic nerves stained with PPD (A–L). All mutants overexpressing PMP22 showed lack of large caliber myelinated fibers, which are depicted in wildtype and MAG-deficient mice (A–C, white star). Small and medium size fibers of those animals manifested either a normal g-ratio (J, arrows) or were hypomyelinated (J, arrowheads). Overall, there was a significant reduction of myelinated fibers in the C22 mouse line (M) compared to wildtype littermates (*, $p<0.0005$). The deletion of MAG in the C22 background did not further decrease the total number of myelinated fibers (*, $p<0.0005$, M). Data are expressed as mean and s.e.m. of three animals at P40. Scale bars: (A–F) 100 μm; (G–L) 10 μm.

per genotype at P4 and P7, and six nerves from three mice ($n=3$) per genotype at P60.

For qRT-PCR, 100 ng total RNA of each sample was reverse transcribed using the SuperScript III Reverse Transcriptase (Invitrogen). qRT-PCR was performed using the Fast SYBR Master Mix Kit (Applied Biosystems) on a 7500 Fast Real-time PCR System (Applied Biosystems) according to the manufacturer's protocol.

qRT-PCR was performed with the same RNA as for the microarray analysis, using the following primers: Necl4/Cadm4: forward, CTGGA ACCGTGGGAATGAGTC; reverse, GGCGTAAGGAACCGATGTCTG; NF155: forward, GGAGGGAAAGCAGTTTGTGAAG; reverse, AATCAGGATTCCGT TGGGGTGCTC; Ngfr/p75^{NTR}: forward, AGCGTGAGGAGGTCGAGAAG; reverse, CATCAGCGGTCGGAATGTGG; ErbB2: forward, GAGCCTTCG GCACTGTCTAC; reverse, GGCAGCCATAGGGCATAAGC; ErbB3: forward, GGCAACTCTCAGGCAGTATGTC; reverse, ACCACTCGGAGGTTAGGTAAGG; JNK: forward, CTTAAAGCCAGTCAGGCAAGA; reverse, TTCCTGCACCTG TGCTAAAG; 60S: forward, GGA AGT ACC AGG CAG TGA CAG; reverse, GCA GGC ATG AGG CAA ACA G. The acquired mRNA copy numbers were normalized to the 60S ribosomal protein subunit L13a. Five experimental samples were investigated for P0, four were used for P4, P7 and P10 and three for P60. For each gene the expression level at particular time point and genotype was normalized to its wildtype P0 level, which was set to 1. Data are shown as mean and s.d.

Results

Complementary expression of MAG and Necl4 in CMT1A patients

To investigate whether MAG and Necl4 expression is altered in CMT1A patients, we performed immunohistochemistry on human tissue samples (Fig. 1). Quantitative immunohistochemical analysis for MAG and myelin protein zero (P0, MPZ) was performed on transversal sections of sural nerves of CMT1A and control cases. In control tissues, MAG was detected in 64% of myelinated fibers, whereas in CMT1A tissue 89% of myelinated fibers were MAG positive (Supplementary Fig. 1G). In addition, the ratio of the positive MAG to positive P0 areas was increased from 0.048 (±0.016 s.e.m.) in controls to 0.311 (±0.15 s.e.m.) in CMT1A patients (Fig. 1I). The relative increase of MAG expression could be confirmed using an alternative set of antibodies recognizing specifically either the long (L-MAG) or short (S-MAG) isoforms

(Figs. 1C,D,G,H). A similar increased ratio of MAG expression was observed in biopsies from HNPP patients (Supplementary Fig. 1).

Immunofluorescent analysis for Necl4, MAG, and P0 was performed on transversal tissue sections of sural nerve biopsies of CMT1A and control cases (Fig. 2). This analysis revealed that Necl4 was strongly decreased in CMT1A nerves when compared to control tissues (Figs. 2E,K). Analyzing single fluorescence profiles through myelinated fibers demonstrated a robust reduction of Necl4 immunofluorescence in CMT1A patients (Figs. 2N,P). Colocalization of Necl4 and MAG in control tissue sections confirmed the overlapping localization of the two proteins in non-compact myelin including periaxonal membranes and Schmidt–Lanterman incisures (Fig. 2I). The intensity profile revealed a high degree of colocalization that is exemplified by the profiles of the fluorescent signals through a single fiber (Fig. 2O). Immunofluorescent analysis of CMT1A nerve tissue showed a strong reduction of Necl4, whereas MAG expression was elevated (Fig. 2P), supporting our original observations (Fig. 1).

Increased MAG and decreased Necl4 expression in a CMT1A animal model

We further investigated the expression of MAG in the C22 mouse line, an animal model for CMT1A disease overexpressing human PMP22 (Huxley et al., 1996), by performing immunofluorescence for MAG on transversal sciatic nerve tissue sections (Figs. 3A–F). For quantification we measured areas positive for MAG and compact myelin proteins PMP22 and P0 within single myelinated fibers in C22 and wildtype mice. This analysis revealed an increase in the ratio of MAG-positive to P0-positive areas (Fig. 3G). Since a pathological landmark of C22 mice is the predominance of small caliber fibers, which generally also express more MAG (Erb et al., 2006), we discriminated between fibers with a diameter larger and smaller than 5 μm in wildtype nerves (Fig. 3G). This comparison also revealed an increase in the MAG/P0 ratio indicating a general increase of MAG expression in C22 peripheral nerves. No general difference in the ratio of PMP22-positive and P0-positive areas could be identified in C22 peripheral nerves (Fig. 3H). Moreover, Western blot analysis of myelin membranes isolated from sciatic nerves confirmed an increased MAG expression in C22 mice (Fig. 3I). In C22 mice, the relative amounts of MAG compared to compact myelin proteins myelin basic protein (MBP) and P0 were strongly elevated. These findings indicate that altered PMP22 expression is associated with an increased MAG expression in CMT1A patients as well as in a mouse model for CMT1A.

Opposite results were obtained by analyzing sciatic nerves of C22 and control mice for Necl4 (Figs. 3K–R). A decrease in Necl4 immunofluorescence was observed in sections from sciatic nerves of adult C22 mice (Fig. 3P), when compared to wildtype mice (Fig. 3L). Furthermore, Western blot analysis revealed a marked decrease in the amount of both Necl4 and Necl1 in nerve extracts from C22 mice compared to wildtype nerves (Fig. 3S). Altogether, we show a decrease of Necl4 expression in CMT1A patients as well as in C22 mice.

Differential expression of Necl4 and MAG during development in C22 mice

As we identified increased expression of MAG and decreased expression of Necl4 in adult C22 mice, we investigated their expression

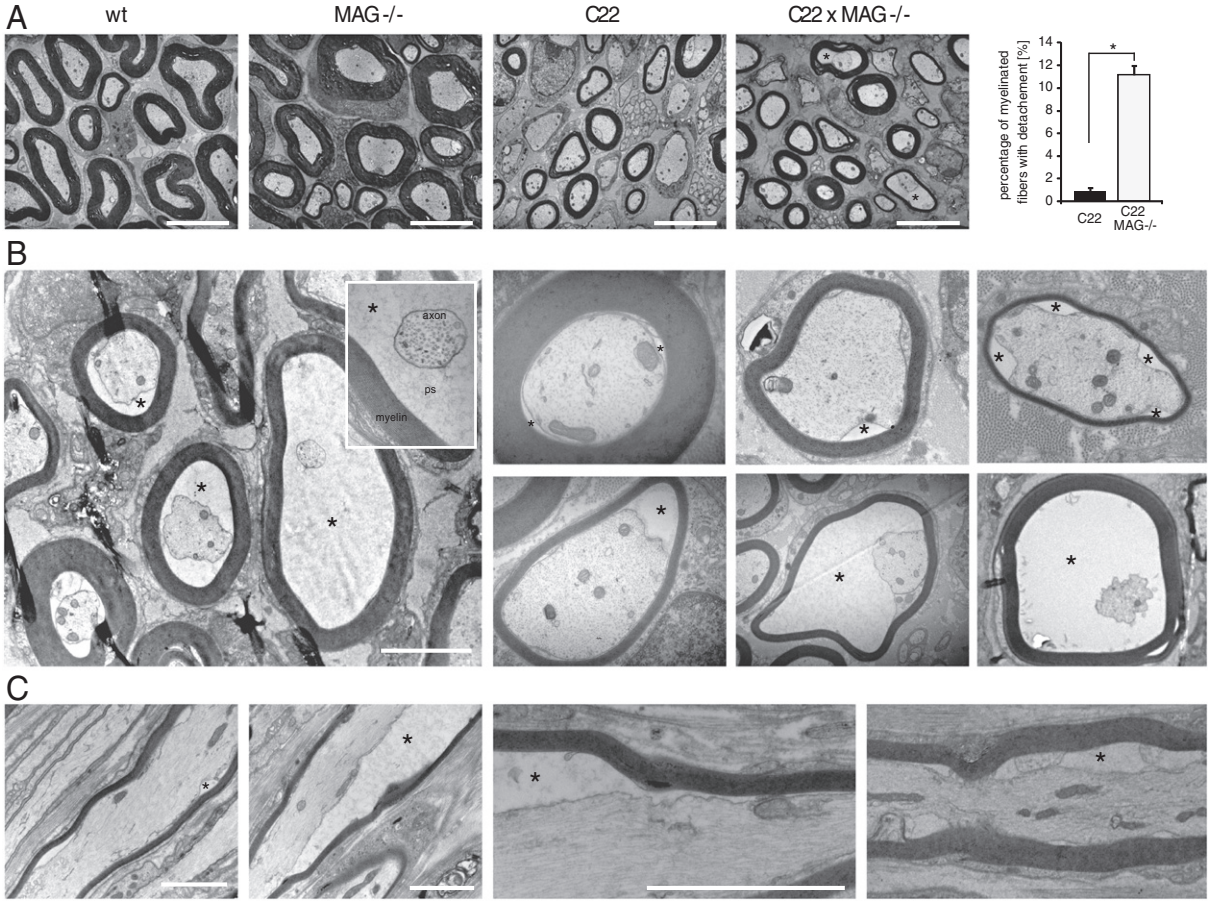

Fig. 5. Loss of axon–glia interaction in MAG-deficient C22 mice. EM micrographs of sciatic nerves from wildtype, MAG–/–, C22, and C22xMAG–/– mice are shown (A). Ultrastructural analysis using electron microscopy revealed a significant number of myelinated fibers with increased periaxonal space in C22xMAG–/– (A, plot and B). Data are shown as mean and s.e.m. of three animals at P40 (*, $p = 0.00022$). Different degrees of axonal detachments from the Schwann cell membrane could be detected (B, asterisk depicts periaxonal space). Longitudinal sections of fibers revealed that within one fiber different degrees of axon detachment can occur (C). First detachments can be observed at the age of P20 (data not shown). Scale bars: (A) 5 μm; (B, C) 2 μm.

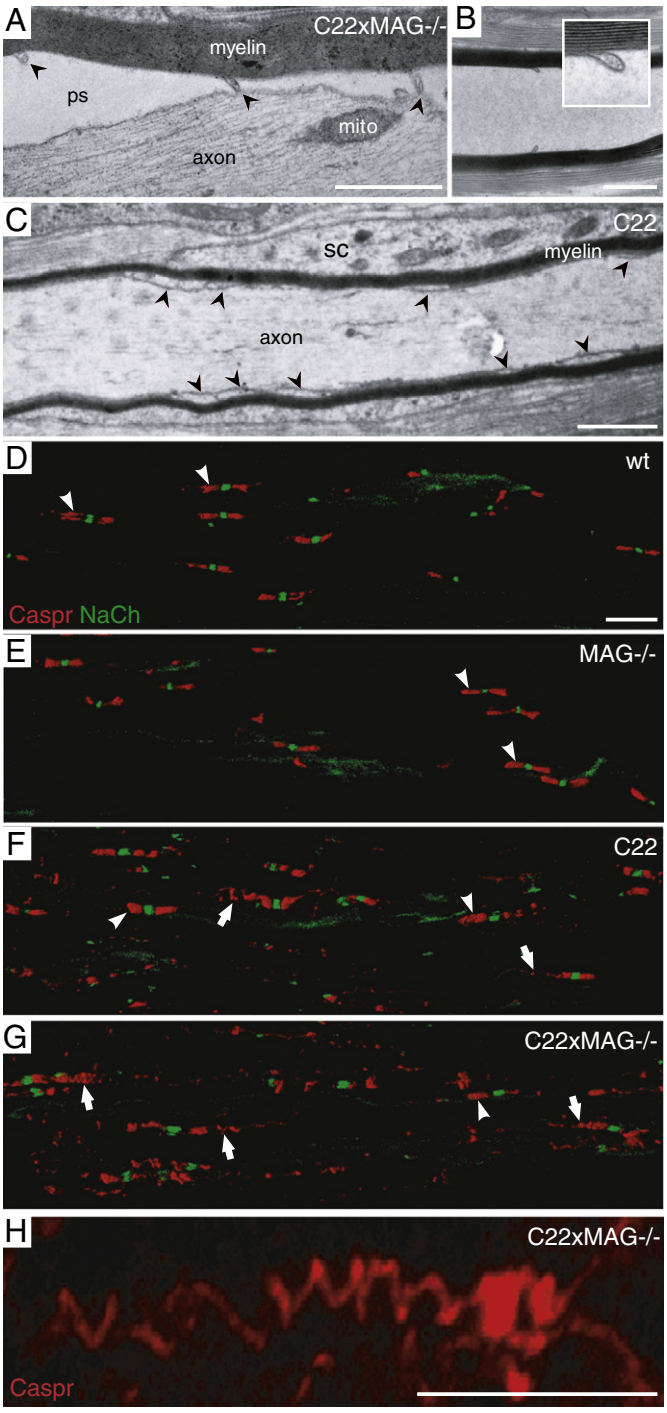

Fig. 6. Ectopically localized loops of the lateral rim in C22 and MAG-deficient C22 mice. Ectopically localized loops of the cytoplasmic rim of the myelin membrane were observed within the internodal region (A, arrowheads; B inset; pictures were taken from animals at P40 as example). These ectopically, normally paranodally localized, loops were often still attached to the axonal membrane, although the inner mesaxon of the internode lost axonal contact (A). In some longitudinal sections they were still present even if no axon was visible (B). In C22 animals, similar phenomenon was observed, showing ectopically localized loops of the lateral rim within the internode (C, arrowheads). Immunofluorescent staining for Caspr revealed a distended spiral structure of its localization over more than 20 μm (G; higher magnification, H), which was never observed in wildtype (D) and MAG-deficient mice (E). In C22 animals normal (F, arrowheads), but also distended Caspr localization could be observed, although not to such an extent as in double mutant mice (G, arrows). Pictures were taken from animals at P48 as example. Scale bars: (A–C) 1 μm; (D–G and H) 10 μm. Abbreviations: ps, periaxonal space; mito, mitochondria, sc, Schwann cell cytoplasm.

pattern during development to identify at which developmental time point the differential expression of the two occurs. We performed quantitative RT-PCR and microarray analysis of peripheral nerves of wildtype and C22 nerves at postnatal day 0 (P0), P4, P7, P10 and P60. Mag and Necl4 showed both reduced mRNA expression levels during early postnatal development (Figs. 3T,U), which is most probably due to the delayed myelination phenotype of these mice. However, in the adult nerves (P60) Mag mRNA expression was upregulated (Fig. 3T), whereas Necl4 mRNA expression stayed very low (Fig. 3U), corresponding to our observations on the protein level (Fig. 3S). The low expression during development was also observed for other myelin genes, such as P0 (Mpz, Fig. 3V), Pmp22, myelin and lymphocyte protein (Mal), and neurofascin 155 (Supplementary Fig. 2B). However at P60, the expression of most of the major myelin genes were increased, achieving in many cases comparable wildtype levels. Beside Mag, we identified gliomedin (Gldn) and myelin protein 11 (Mp11) to be upregulated in mature C22 nerves (Supplementary Fig. 2A), indicating a general disturbance of the axon–glia interaction to which MAG, gliomedin and MP11 might react. In summary, the expression analysis revealed a failure in Necl4 expression induction, despite the fact that transcription factors essential for terminal differentiation of Schwann cells and initiation of myelination are comparably expressed in C22 mice (Supplementary Fig. 2C).

MAG expression in C22 mice is essential

Our data show that the molecular composition of the axon–glia interface is altered in the CMT1A disease, and that the increase of MAG might be a compensatory reaction. To test whether MAG has a beneficial protective effect in PMP22-overexpressing mice, we crossed MAG-deficient mice with C22 mice. C22 mice display a tremor that is visible after three weeks (Huxley et al., 1996), but do not show increased lethality up to 6 months (data not shown). The MAG-deficient mice exhibit no abnormal behavioral phenotype and have a normal life expectancy (Montag et al., 1994). In contrast to the single mouse lines (C22, MAG−/−), the C22xMAG−/− double mutants are often smaller than their single mutant littermates (Supplementary Figs. 3A,B) and have a reduced life expectancy (Supplementary Fig. 3C), which was never observed for any single mouse line (data not shown). In the hind limbs, they have a slightly more pronounced tremor phenotype and show occasionally myotonia-like contractions, which become evident at an age of three weeks. However, investigation of neuromuscular junctions of the soleus, sternomastoid and tibialis muscles did not reveal differences between C22 and C22xMAG−/− double mutant mice (data not shown). Western blot analysis confirmed the expected combination of reduced expression of Necl4 in C22 mice and the complete absence of MAG in the C22xMAG−/− double mutants (Supplementary Fig. 3D). Western blot analysis with antibodies against myelin proteins revealed that there was no further reduction of myelin protein levels in double C22xMAG−/− mutants compared to the single C22 mice. Our data raise the possibility that the increase in MAG expression in C22 mice may have a compensatory effect for the reduction of Necl4.

Loss of axon–glia interaction in C22xMAG−/− mutant mice

We further investigated if the loss of MAG in the double C22xMAG−/− mutant mice leads to myelin alteration. First, we analyzed the morphology of sciatic nerves using semi-thin transverse sections stained for myelin with p-phenylenediamine (PPD) at P40 (Fig. 4). C22, C22xMAG+/− and C22xMAG−/− mice lack large caliber myelinated fibers (Huxley et al., 1996), which are present in wildtype and MAG-deficient nerves (Figs. 4A–C, white star). However, C22 mice have around 50% normal small and medium myelinated fibers (Fig. 4J, arrows), and about 30% hypomyelinated fibers (Fig. 4J, arrowheads). Still, a comparable number of axons in C22 nerves was observed when compared to wildtype mice (data not shown). A significant reduction in myelinated fibers was observed in C22 mice (61% reduction

compared to wildtype mice, $p = 0.00011$) or in double mutants (51% reduction compared to wildtype mice, $p = 0.0055$). C22 mice lacking MAG did not show significant alterations in the total number of myelinated fibers compared to C22 mice (Fig. 4M), nor in fiber caliber and myelin thickness (Figs. 4J–L). However, in the double mutants some unusual large fiber profiles were noticeable (Fig. 4L, arrowhead). We further analyzed the morphology on ultrastructural level using electron microscopy (Fig. 5). The most conspicuous difference in the double mutants compared to wildtype as well as single mutants was the detachment of the axon membrane visible by the enlargement of the periaxonal space (Fig. 5B, asterisk). Axon–glia detachments were defined as regions where the membrane of the axon was not in direct contact with the membrane of the myelinating Schwann cell. Several degrees of detachments could be observed. Some fibers show only partial contact loss and others exhibit a total detachment without any direct contact between axon and Schwann cell membrane (Fig. 5B). A significant proportion of 11.22% ($\pm$0.44% s.e.m., $p = 0.00022$) of myelinated fibers in the double mutant showed signs of detachment (Fig. 5a, plot), whereas in C22 animals this phenomenon was only detectable in less than 1% of myelinated fibers (0.83% $\pm$ 0.20% s.e.m.), and never to the extent observed in double mutant mice. Occasionally, some axon profiles were separated from the inner aspect of their myelin sheath in MAG-deficient mice comparable to the observations described previously (Li et al., 1994), but this event was rare and might be attributed to a fixation artefact (Li et al., 1994). The analysis of these enlarged periaxonal profiles in longitudinal sections revealed that the degree of detachment could vary along the length of one fiber (Fig. 5C). Investigation of the relation between the inner fiber diameter and the myelin sheath thickness of detached fibers revealed that the caliber of a number of detached fibers is too large for their myelin sheath thickness. The mean ratio of the inner to the total fiber diameter was 0.75 ($\pm$0.08 s.d.). It varies between normal fibers with a ratio of around 0.65 (comparable to wildtype mice) and hypomyelinated ones with a ratio of around 0.75 (comparable to C22 mice). Still, a number of fibers had a ratio of up to 0.92, which is even higher than ever observed in C22 mice. These fibers with unusual large caliber were already identified at low magnification (Fig. 4L, arrowhead).

Ectopically localized loops of the lateral rim in C22 and MAG-deficient C22 mice

The analysis of longitudinal sections revealed also ectopically localized loops of the lateral cytoplasmic rim along the internode that were not obviously associated with a nodal structure (displaced "paranodal loops"; Figs. 5C, 6A, arrowhead); some of them were still associated with the axon (Fig. 6A), others were not (Fig. 6B). The phenomenon of ectopically localized loops of the lateral rim of a myelin lamella could also be observed in C22 mice (Fig. 6C, arrowheads), suggesting that in C22 mice the paranodal organization of the node of Ranvier is already impaired. Immunofluorescent analysis of Caspr, a marker for paranodes (Gollan et al., 2003) (Fig. 6D, arrowheads), revealed that the axonal paranodal structure in C22 (Fig. 6F, arrows) and double mutant (Fig. 6G, arrows) mice is impaired as well. Caspr immunofluorescent indicated that most of the paranodes show a strong dislocated spiral-like pattern (Figs. 6G, arrows, H), which was already evident in C22 mice (Fig. 6F, arrows), and never observed in MAG-deficient (Fig. 6E, arrowheads) and in wildtype mice (Fig. 6D, arrowheads), even though a comparable sodium channel distribution was observed. Measurements of the area of Caspr immunofluorescence in relation to the number of sodium channel clusters, with which they were associated, revealed a prominent increase of paranodal Caspr-positive area in C22 compared to wildtype and MAG-deficient mice (data not shown). Our data is in line with earlier observations in the trembler mouse, another CMT1A animal model, in which disorganization of paranodal restriction of Caspr was observed (Devaux and Scherer, 2005). We did not observe any signs of axonal degeneration or pathological alterations of detached axons. The neurofilament density did not increase as it is usually the case in "demyelinated" axons, nor accumulation of intracellular components indicative of impaired axonal transport could be observed. In summary, the ultrastructural analysis of the C22xMAG−/− mutant revealed strong axonal attachment defects of the inner mesaxon underlining the importance of MAG and Necl4 as essential factors for maintaining the axon–glia interaction.

Discussion

Charcot–Marie–Tooth type 1A (CMT1A) disease is a hereditary demyelinating neuropathy. It is caused by either an overexpression or a mutation in the PMP22, which causes a disturbance in the normal function of Schwann cells. One of the commonly used mouse models, the C22 mouse line overexpressing human PMP22 (Huxley et al., 1996), develop a very similar disease course characterized by dysmyelination and axonal pathologies consisting of decreased axonal calibers, decreased nearest neighbor distances of neurofilaments and a decreased phosphorylation state of neurofilament subunits (Cole et al., 1994; de Waegh et al., 1992; Nobbio et al., 2006), but it should be noted that it does not show all features of myelin destruction and onion bulb formation as observed in CMT1A patients. Molecular candidates involved in axon–glia interactions are MAG and Necl4, expressed by Schwann cells and localized in particular myelin sheath compartments such as periaxonal membranes and paranodal loops (Erb et al., 2006; Spiegel et al., 2007; Trapp, 1990). We found a robust upregulation of MAG protein in nerve biopsies of CMT1A patients, whereas Necl4 was almost absent. Investigations of C22 mice confirmed the upregulation of MAG and strong reduction of Necl4 protein. Further analysis showed that MAG was mainly localized in periaxonal membranes, Schmidt–Lanterman incisures and paranodes, similar to wildtype mice. The strong reduced expression of both Necl4 and Necl1 in C22 mice makes them likely candidates important for Schwann cell mediated axonal pathology in CMT1A. Reduced Necl4 expression in peripheral nerves of CMT1A patients and the corresponding mouse model strengthen a possible involvement of Necl4 in CMT1A pathology. Since Necl4-deficient mice do not exhibit the same degree of delayed myelination as C22 mice (data not shown), we investigated the transcriptional expression pattern of Necl4 during peripheral nerve development. At birth, Necl4 and MAG had comparable expression patterns in C22 and wildtype mice. During the first two postnatal weeks their expression was reduced in C22 nerves compared to wildtype nerves, resembling the delayed onset of myelination. The discrepancy between the two occurs during the maturation phase; MAG is upregulated whereas Necl4 expression remains low. From these gene expression data we assume a dysregulation in Schwann cells of C22 mice leading to Necl4 downregulation during myelin maturation. Indeed, a comprehensive expression analysis revealed a whole set of genes differentially expressed in mature C22 nerves (Supplementary Fig. 2). Interestingly, genes involved in terminal differentiation and initiation of myelination such as transcription factors Krox20/Egr2, Oct6/SCIP, and neurotrophin and neuregulin receptors were not altered during early development. This is surprising as many genes, whose initiation is thought to be dependent on Krox20/Egr2 (Nagarajan et al., 2001) such as Mpz, Mal, Pmp22, were expressed at very low levels, whereas others such as for example $p75^{NTR}$, Sox2, Krox24/Egr1, Sox10 and c-jun were expressed at wildtype levels (Supplementary Fig. 2). However, a difference in the expression pattern could be detected for one of the coactivators, namely Nab1 (Supplementary Fig. 2A). The Nab proteins, Nab1 and Nab2, can interact and modulate Krox20/Egr2 activity, and are known to be essential for Krox20/Egr2-mediated myelination (Le et al., 2005; Mager et al., 2008; Srinivasan et al., 2007). Mice lacking Nab1 and Nab2 develop severe congenital hypomyelination of peripheral nerves, and Schwann cells arrest in the premyelinating stage, despite the fact that Krox20/Egr2 is normally expressed (Le et al., 2005). In contrast to Nab1, which has a comparable expression pattern to Necl4, Nab2 expression was not changed in C22 mice. As for many myelin genes, Nab1 expression is also steadily increasing during normal postnatal

development, whereas Nab2 expression seems to stay on a relative constant level (Supplementary Fig. 2). Earlier studies indicated that Krox20/Egr2 is directly involved in the regulation of Nab1 expression, since Krox20/Egr2-deficient mice showed reduced expression of Nab1, but not of Nab2 (Srinivasan et al., 2007). From our study we have to assume that reduced Nab1 expression does occur despite normal Krox20/Egr2 expression, although we cannot conclude whether the whole transcriptional activation machinery of Krox20/Egr2 is fully functional. One of the observed discrepancy might be that the level of Nab1 expression directly influences the degree of promoter activation by Krox20/Egr2-dependent genes; for particular myelin genes little activation is already enough (e.g. Mbp, Krox24/Egr1, $p75^{NTR}$, and ErbB2/3), and this might be sufficient for small caliber fiber myelination. However, other myelin genes might need a threshold level of Nab1 for their full activation (e.g. Mpz, Pmp22, Mal, and Necl4), that might be more crucial for large caliber fiber. Although Nab1-deficient mice appeared grossly normal, a tendency to hypomyelination during postnatal development might be possible (Figure 3l in Le et al., 2005).

To investigate if MAG has a protective function in the CMT1A mouse model, we generated C22 mice deficient for MAG. A significant number of double mutants die after several weeks identifying MAG as a protective factor in CMT1A. This is supported by a recent study demonstrating a protective effect of MAG on axons in experimental induced axon degeneration models (Nguyen et al., 2009). Ultra structural analysis using electron microscopy revealed a severe defect in axon–glia interaction of MAG-deficient C22 mice. Detachment of the axon from the inner mesaxon of the Schwann cell was observed in the double mutants, but very seldom in C22 and rarely in MAG-deficient mice. This suggests that in CMT1A the axon–glia interaction is already disturbed and the increase in MAG has a protective effect in maintaining axon–glia adhesion. Depletion of MAG in the CMT1A animal model may lead to a further reduction of the adhesive properties of the axon–glia interface (Supplementary Fig. 4). This reduction leads finally to an uncoupling of the axon from the myelin sheath (Supplementary Fig. 4A), suggesting that a tight interaction between myelin and axon is necessary for the coordinate growth and maintenance of myelin and axons. We observed that most fibers with total loss of axon–glia interaction have small axons. This could be explained by a secondary retraction of the axon (Supplementary Fig. 4BI), by an uncoordinated growth of the myelin sheath (Supplementary Fig. 4BIII) or both (Supplementary Fig. 4BII). One mechanism by which MAG is involved in the coordinated growth of a myelinated axon would be that the MAG molecules are attachment sites to pin the axon to the myelin sheath. One could speculate that the spiral myelin sheath could act like a mainspring and produces a stretching force on the anchored axon important for the coordinated growth. Lack of adhesion would therefore lead to the detachments seen in double mutants (Supplementary Fig. 4C).

Although MAG and Necl4 have an overlapping expression pattern, there is a difference which might be of interest in this context. Periaxonal MAG expression is mainly observed in small and medium caliber fibers, whereas in large caliber fibers MAG expression is predominant in Schmidt–Lanterman incisures (Erb et al., 2006). This is in contrast to Necl4 which is localized within the periaxonal membrane of all myelinated fibers (Spiegel et al., 2007). In C22 mice large caliber fibers are not myelinated, but remain in a 1:1 relationship with the Schwann cell. This might be due to the strong reduction of Necl4, as functional disruption of Necl4 in in vitro myelinating DRG/ Schwann cells co-cultures have shown to block myelination at this particular stage (Spiegel et al., 2007). MAG upregulation might compensate the lack of Necl4 in small and medium caliber fibers to some extent, but is not able to accomplish it in large caliber fibers. Deficiency of MAG in C22 mice did not reveal a further dysmyelinating phenotype, which was not unexpected since it was shown before that myelination in MAG-deficient mice is not severely impaired. However, a detachment of the myelin sheath from the axon becomes only evident when MAG was abolished. This demonstrates the importance of MAG in glial adhesion to the axon. In the CMT1A disease, increased MAG might have a compensatory role to counteract reduced axon–glia adhesion to which the reduction of Necl4 may contribute. Necl4 might have an overlapping role in myelination and adhesion, which each one can compensate the other to some extent.

In summary, our data show a marked alteration of the molecular composition of the axon–glia interface in CMT1A, identifying a novel and major pathogenic mechanism in this disease. This is prominently shown by the downregulation of Necl4, an adhesion molecule involved in myelination. Further, the observed upregulation of MAG in CMT1A suggests a vital compensatory mechanism for maintaining the axon–glia integrity. Thus, we demonstrated that MAG together with other adhesion molecules such as Necl4 is important in supporting axonal integrity. A better understanding of the mechanisms involved in the regulation of the expression of these adhesion molecules will open new therapeutical approaches to the treatment of demyelinating neuropathies.

Contributors

J.K., T.L., T.Z., D.S., B.E., R.L. performed the experiments and analyzed the data; A.J.S. and N.S.W. supervised the study; R.L. and B.E. made the initial observation; J.K. and T.L. did most of the experiments and compiled the data; R.L. and B.E. made the experiments involving the CMT1A and HNPP patients; J.K., B.E. and T.L. made the experiments involving confocal and EM microscopy of CMT1A patients and C22 mice; T.Z. and D.S. made the differential expression analysis; A.J.S. and D.P. provided human nerve tissues; E.P. provided instrumental feedback on the manuscript; and J.K. and N.S.W. wrote the manuscript.

Supplementary data to this article can be found online at http://dx.doi.org/10.1016/j.nbd.2012.08.009.

Acknowledgments

Thanks goes to Dr. Bettina Geidl-Flück (Neurobiology, Department of Biomedicine, Basel, Switzerland) for her experimental contribution, to Dr. Alphonse Probst (Neuropathology, University Hospital Basel, Switzerland) for providing control autopsies, to Dr. Clare Huxley (Division of Biomedical Sciences, Imperial College School of Science, London, UK) for providing the PMP22 overexpressing mice, to Dr. Klaus Armin Nave (MPI Göttingen, Germany) for providing the MAG knockout mice, to Dr. Leda Dimou (Institute for Physiology, Ludwig-Maximilians-Universität, Munich, Germany) for providing some MAG knockout tissues, Dr. Ueli Certa (Molecular Toxicology, Pharmaceutical Divison, F. Hoffmann-La-Roche AG, Basel, Switzerland) for access to the microarray facility and technical support, and to Dr. Hans-Rudolf Brenner and Dr. Nadine Schmidt (Institute for Physiology, University of Basel, Switzerland) for the analysis of the neuromuscular junction. This work was supported by the Swiss National Science Foundation (to NSW 3100A 0-112583) and the NIH (NINDS grant NS50220 to EP).

References

Bartsch, U., 2003. Neural CAMS and their role in the development and organization of myelin sheaths. Front. Biosci. 8, d477–d490.
Bartsch, U., et al., 1995. Multiply myelinated axons in the optic nerve of mice deficient for the myelin-associated glycoprotein. Glia 14, 115–122.
Berciano, J., et al., 1989. The application of nerve conduction and clinical studies to genetic counseling in hereditary motor and sensory neuropathy type I. Muscle Nerve 12, 302–306.
Bouche, P., et al., 1983. Peroneal muscular atrophy. Part 1. Clinical and electrophysiological study. J. Neurol. Sci. 61, 389–399.
Burger, D., et al., 1990. The epitope(s) recognized by HNK-1 antibody and IgM paraprotein in neuropathy is present on several N-linked oligosaccharide structures on human P0 and myelin-associated glycoprotein. J. Neurochem. 54, 1569–1575.
Cole, J.S., et al., 1994. Modulation of axon diameter and neurofilaments by hypomyelinating Schwann cells in transgenic mice. J. Neurosci. 14, 6956–6966.
de Waegh, S.M., et al., 1992. Local modulation of neurofilament phosphorylation, axonal caliber, and slow axonal transport by myelinating Schwann cells. Cell 68, 451–463.
Devaux, J.J., Scherer, S.S., 2005. Altered ion channels in an animal model of Charcot–Marie–Tooth disease type IA. J. Neurosci. 25, 1470–1480.

Erb, M., et al., 2006. Unraveling the differential expression of the two isoforms of myelin-associated glycoprotein in a mouse expressing GFP-tagged S-MAG specifically regulated and targeted into the different myelin compartments. Mol. Cell. Neurosci. 31, 613–627.
Eshed, Y., et al., 2005. Gliomedin mediates Schwann cell–axon interaction and the molecular assembly of the nodes of Ranvier. Neuron 47, 215–229.
Gabriel, J.M., et al., 1997. Gene dosage effects in hereditary peripheral neuropathy. Expression of peripheral myelin protein 22 in Charcot–Marie–Tooth disease type 1A and hereditary neuropathy with liability to pressure palsies nerve biopsies. Neurology 49, 1635–1640.
Garcia, A., et al., 1998. Charcot–Marie–Tooth disease type 1A with 17p duplication in infancy and early childhood: a longitudinal clinical and electrophysiologic study. Neurology 50, 1061–1067.
Gollan, L., et al., 2003. Caspr regulates the processing of contactin and inhibits its binding to neurofascin. J. Cell Biol. 163, 1213–1218 (Epub 2003 Dec 15).
Hannila, S.S., et al., 2007. Therapeutic approaches to promoting axonal regeneration in the adult mammalian spinal cord. Int. Rev. Neurobiol. 77, 57–105.
Huxley, C., et al., 1996. Construction of a mouse model of Charcot–Marie–Tooth disease type 1A by pronuclear injection of human YAC DNA. Hum. Mol. Genet. 5, 563–569.
Jessen, K.R., Mirsky, R., 2005. The origin and development of glial cells in peripheral nerves. Nat. Rev. Neurosci. 6, 671–682.
Krajewski, K.M., et al., 2000. Neurological dysfunction and axonal degeneration in Charcot–Marie–Tooth disease type 1A. Brain 123 (Pt 7), 1516–1527.
Le, N., et al., 2005. Nab proteins are essential for peripheral nervous system myelination. Nat. Neurosci. 8, 932–940.
Li, C., et al., 1994. Myelination in the absence of myelin-associated glycoprotein. Nature 369, 747–750.
Mager, G.M., et al., 2008. Active gene repression by the Egr2.NAB complex during peripheral nerve myelination. J. Biol. Chem. 283, 18187–18197 (Epub 2008 May 2).
Martini, R., 2001. The effect of myelinating Schwann cells on axons. Muscle Nerve 24, 456–466.
Martini, R., Schachner, M., 1986. Immunoelectron microscopic localization of neural cell adhesion molecules (L1, N-CAM, and MAG) and their shared carbohydrate epitope and myelin basic protein in developing sciatic nerve. J. Cell Biol. 103, 2439–2448.
Maurel, P., et al., 2007. Nectin-like proteins mediate axon Schwann cell interactions along the internode and are essential for myelination. J. Cell Biol. 178, 861–874.
Miescher, G.C., et al., 1997. Reciprocal expression of myelin-associated glycoprotein splice variants in the adult human peripheral and central nervous systems. Brain Res. Mol. Brain Res. 52, 299–306.
Miller, S.L., et al., 1984. Production and characterization of monoclonal antibodies to peripheral and central nervous system myelin. J. Neurochem. 43, 394–400.
Montag, D., et al., 1994. Mice deficient for the myelin-associated glycoprotein show subtle abnormalities in myelin. Neuron 13, 229–246.
Nagarajan, R., et al., 2001. EGR2 mutations in inherited neuropathies dominant-negatively inhibit myelin gene expression. Neuron 30, 355–368.
Nave, K.A., Salzer, J.L., 2006. Axonal regulation of myelination by neuregulin 1. Curr. Opin. Neurobiol. 16, 492–500 (Epub 2006 Sep 7).
Nave, K.A., Trapp, B.D., 2008. Axon–glial signaling and the glial support of axon function. Annu. Rev. Neurosci. 31, 535–561.
Nelis, E., et al., 1996. Estimation of the mutation frequencies in Charcot–Marie–Tooth disease type 1 and hereditary neuropathy with liability to pressure palsies: a European collaborative study. Eur. J. Hum. Genet. 4, 25–33.
Nguyen, T., et al., 2009. Axonal protective effects of the myelin-associated glycoprotein. J. Neurosci. 29, 630–637.
Nicholson, G.A., 1991. Penetrance of the hereditary motor and sensory neuropathy Ia mutation: assessment by nerve conduction studies. Neurology 41, 547–552.
Nobbio, L., et al., 2006. Axonal damage and demyelination in long-term dorsal root ganglia cultures from a rat model of Charcot–Marie–Tooth type 1A disease. Eur. J. Neurosci. 23, 1445–1452.
Patel, P.I., et al., 1992. The gene for the peripheral myelin protein PMP-22 is a candidate for Charcot–Marie–Tooth disease type 1A. Nat. Genet. 1, 159–165.
Poliak, S., et al., 1999. Caspr2, a new member of the neurexin superfamily, is localized at the juxtaparanodes of myelinated axons and associates with K+ channels. Neuron 24, 1037–1047.
Roa, B.B., et al., 1991. Charcot–Marie–Tooth disease type 1A: molecular mechanisms of gene dosage and point mutation underlying a common inherited peripheral neuropathy. Int. J. Neurol. 25–26, 97–107.
Schaeren-Wiemers, N., et al., 2004. The raft-associated protein MAL is required for maintenance of proper axon–glia interactions in the central nervous system. J. Cell Biol. 166, 731–742.
Schenone, A., Mancardi, G.L., 1999. Molecular basis of inherited neuropathies. Curr. Opin. Neurol. 12, 603–616.
Sereda, M.W., Nave, K.A., 2006. Animal models of Charcot–Marie–Tooth disease type 1A. Neuromolecular Med. 8, 205–216.
Spiegel, I., et al., 2007. A central role for Necl4 (SynCAM4) in Schwann cell-axon interaction and myelination. Nat. Neurosci. 10, 861–869.
Srinivasan, R., et al., 2007. Differential regulation of NAB corepressor genes in Schwann cells. BMC Mol. Biol. 8, 117.
Suter, U., et al., 1992. Trembler mouse carries a point mutation in a myelin gene. Nature 356, 241–244.
Trapp, B.D., 1990. Myelin-associated glycoprotein. Location and potential functions. Ann. N. Y. Acad. Sci. 605, 29–43.

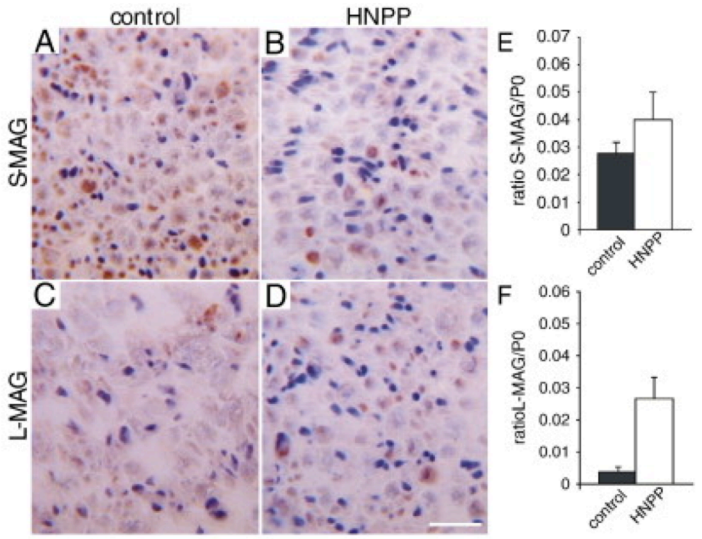

G

		% MAG positive myelinated fibers	ratio MAG/P0	ratio S-MAG/P0	ratio L-MAG/P
Control (S)		50%	0.0774	0.0216	0.0029
Control (U)		79%	0.0454	0.0352	0.0065
Control (X)		64%	0.0212	0.0268	0.0015
CMT1A (mi5)		92%	0.1109	0.0409	0.0505
CMT1A (mi6)		88%	0.2124	0.0723	0.0468
CMT1A (mi7)		87%	0.6105	0.0533	0.0483
HNPP (mi1)		84%	0.1411	0.0232	0.0024
HNPP (mi2)		15%	0.0763	0.0117	0.0261
HNPP (mi3)		61%	0.2027	0.0685	0.0431
HNPP (mi4)		86%	0.3469	0.0410	0.0319
HNPP (mi9)		90%	0.1441	0.0548	0.0301
average values					
Control	(n=3)	64%	0.0480 (0.0163)	0.0279 (0.0040)	0.0036 (0.0
CMT1A	(n=3)	89%	0.3113 (0.1525)	0.0555 (0.0091)	0.0485 (0.0
HNPP	(n=5)	67%	0.1822 (0.0458)	0.0398 (0.0103)	0.0267 (0.0

Supplementary Fig. 1. Quantitative analysis of MAG expression in sural nerves of control, CMT1A and HNPP patients using different antibodies.Transversal sections from sural nerves of control autopsies (A, C) and HNPP biopsies (B, D) were stained for MAG using an antibody against S-MAG (A, B) and an antibody against L-MAG (C, D). Quantitative measurements revealed an increase in the MAG versus P0 ratio in sural nerves of HNPP patients compared to control subjects (E, F). Measured values and calculated ratios for all anti-MAG antibodies from control, CMT1A and HNPP patients used in this study are shown in (G). Data are shown as means ± s.e.m. Scale bar: 20 μm.

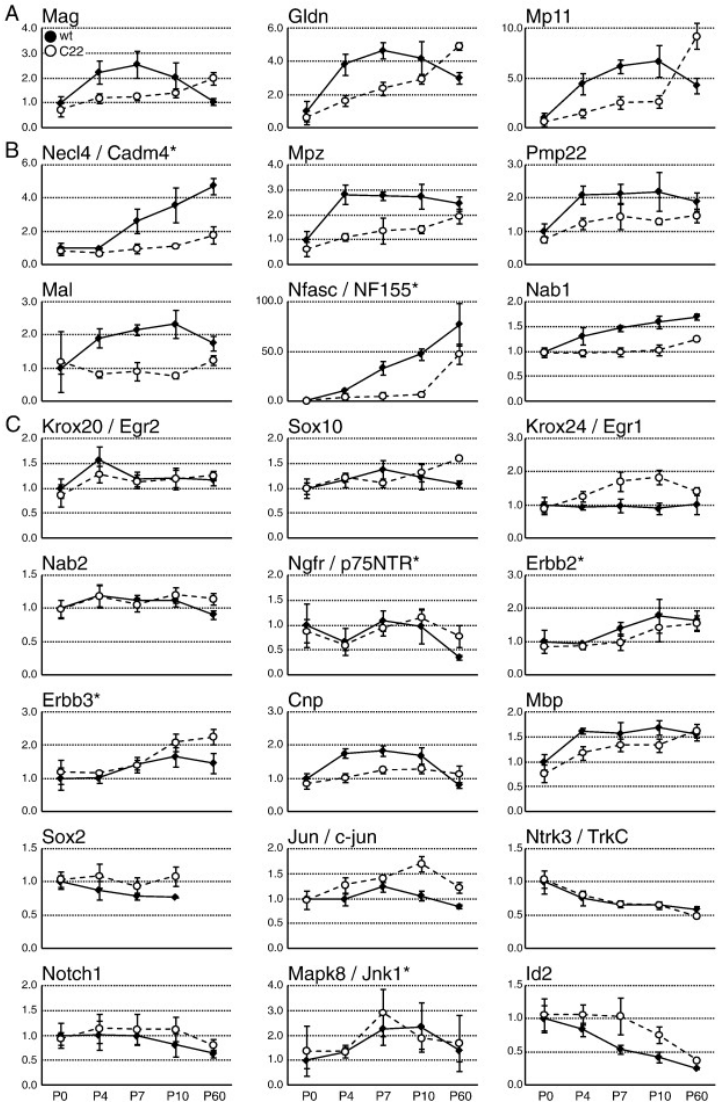

Supplementary Fig. 2. Expression analysis of peripheral nerves during development and in the adult of C22 and wildtype mice.A differential expression analysis was performed by microarray. For genes, which were either not detected by or not present on the microarray, gene expression levels were determined by quantitative RT-PCR (labeled with asterisk). Relative mRNA expression levels at postnatal day 0 (P0), P4, P7, P10 and P60 from wildtype (closed circles) and C22 mice (open circles) were investigated. Gene expression was normalized to the global median (microarray), respectively to the 60S ribosomal protein subunit L13a (quantitative RT-PCR), and thereafter to its wildtype P0 expression level, which was set to 1. Most of the myelin genes showed a delayed expression pattern in C22 during postnatal development, but were either induced in C22 at P60 such as MAG, Gliomedin and MP11 (A) or reduced such as Necl4 and Nab1 (B) or not altered such as MPZ, PMP22, MAL and neurofascin155 (B). The major transcription factors (Krox20, Sox10, Krox24, Nab2) and signaling receptors ($p75^{NTR}$, ErbB2/3) for initiation of myelination, but also the myelin genes CNPase and MBP were not changed in C22 nerves (C). The expression pattern of known negative regulators of myelination such as Sox2 (no expression could be detected at P60), c-jun, Notch1, JNK1, Id2 and TrkC were not significantly altered in C22 nerves during early development (D). Note that expression changes were generally higher in qRT-PCR derived time courses. Nevertheless, the expression profile from qRT-PCR and microarray analysis was comparable. In C22 mice, enhanced proliferation of Schwann cells occurs during late postnatal development, therefore increased expression levels of particular genes involved in Schwann cell proliferation can be depicted at P60 (e.g. Sox10, ErbB3, and c-jun). Data are shown as mean values and standard deviation (s.d.).

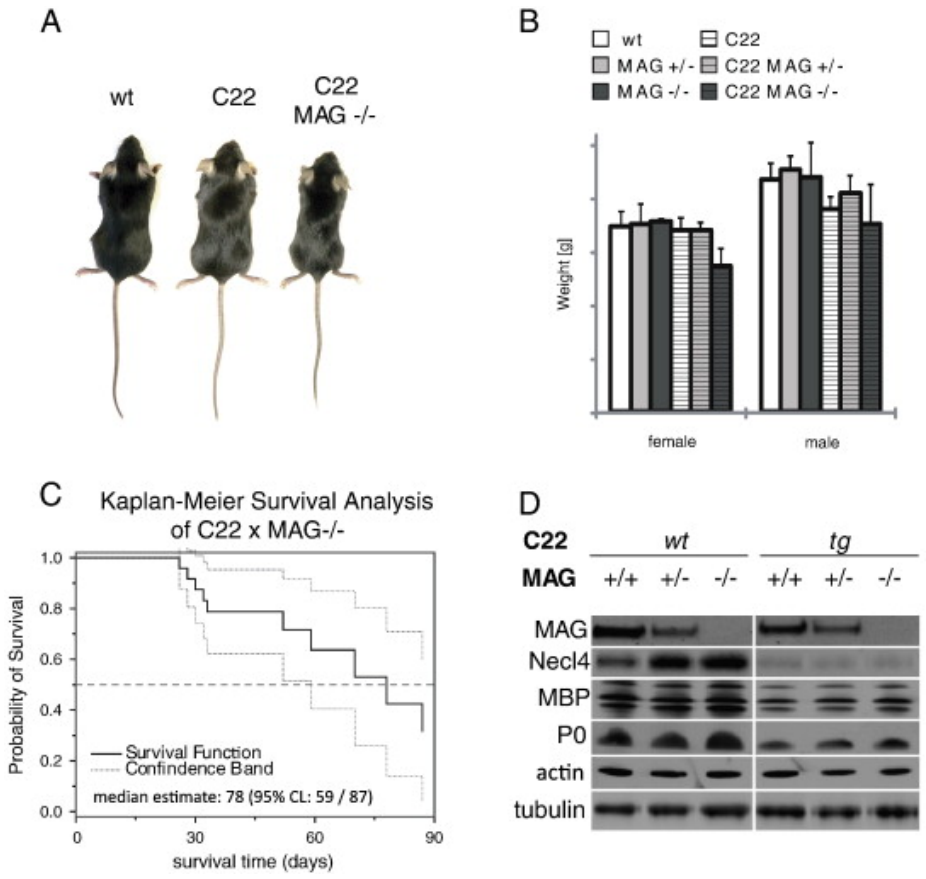

Supplementary Fig. 3. MAG deficiency in the animal model of CMT1A leads to a lethal phenotype.MAG deficient mice were crossbred with C22 mice. Double mutant mice were smaller (A) and had a reduced body weight (B). The results of the quantitative measurements are expressed as mean body weight at six weeks of age for all genotypes and standard deviation (s.d.). 50% of C22 mice homozygous for MAG deletion died between 30 and 80 days after birth (C). All other mice (wildtype, C22, or C22xMAG+/−) do not show increased lethality within six months (not shown). Western blot analysis of all six different genotypes confirms the strong reduction of Necl4 and the loss of MAG protein in the double mutant (C22xMAG−/−) mice (D). Note that the increased MAG expression in C22 was less pronounced in whole nerve protein extracts than in myelin membrane preparations (Fig. 3I). The increase of Necl4 in MAG heterozygous and homozygous mice may point to a compensatory mechanism.

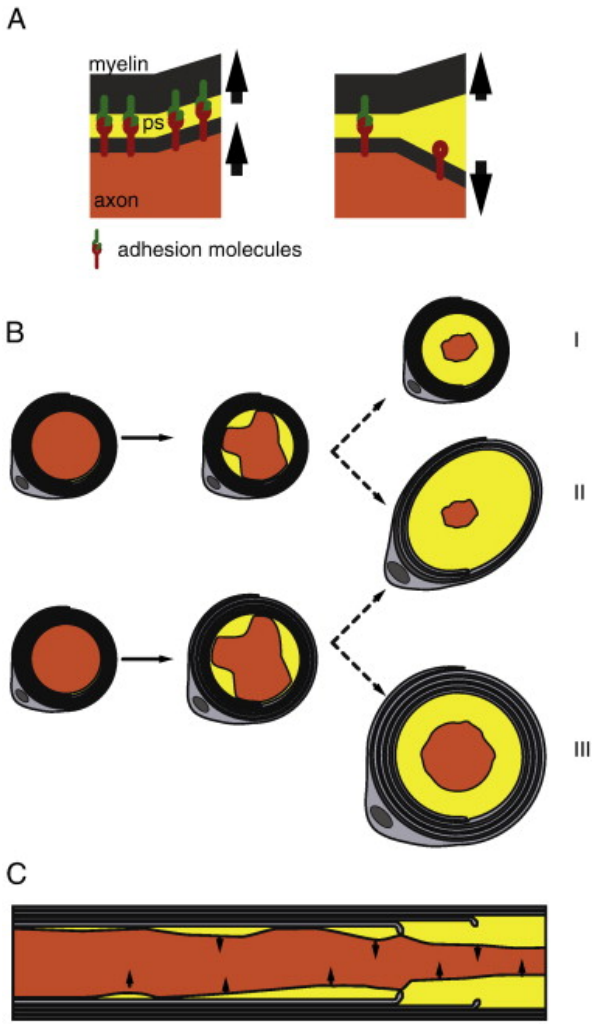

Supplementary Fig. 4. Schematic view of a hypothetical mechanism leading to dissociation of axon and myelin in fibers deficient of adhesion molecules such as MAG and Necl4.A tight interaction mediated by adhesion molecules is important for coordinated growth and the maintenance of the myelinated fiber (A). The axon is tightly associated by adhesion molecules, such as MAG and Necl4, to the myelin sheath. Reduction or loss of adhesion molecules leads to decreased axon–glia interaction and the growth of myelin and axon becomes uncoupled, resulting in disruption of the axon–glia interface and an increase of the periaxonal space (A). One possible mechanism causing an increase of the periaxonal space might be the loss of the axon anchorage to the myelin sheath, leading to the collapse of axon membrane from the inner mesaxon. This "peeling off mechanism" results in further retraction and eventually to an atrophic axon, with relatively a small axon diameter in relation to the myelin thickness (B,I). Another mechanism could involve the continuous growth of the myelin sheaths despite the loss of axon contact (B,III). The lack of adhesive forces might stop axon, growth and therefore, the periaxonal space separating myelin from the axon increases. Alternatively, both mechanisms, an uncoordinated myelin growth and axon retraction, might occur (B,II). The degree of axon–glia detachment within one internode can vary. Ectopical paranodal loops can be detected in internodal regions (C). The specific expression of several adhesion molecules in paranodal loops is responsible for the axon–glia interaction. This distinct subset of adhesion molecules seems to be responsible for the stronger adhesive forces seen in ectopical paranodal loops in the double mutant (C).